Compositional effects in Titan's thermospheric gravity waves

J. Cui,[1] Y. Lian,[3] and I. C. F. Müller-Wodarg[3]

Received 14 November 2012; accepted 5 December 2012; published 16 January 2013.

[1] In Titan's upper atmosphere, the density profiles of several constituents (N_2, CH_4, H_2, and $^{29}N_2$) as measured by the Cassini Ion Neutral Mass Spectrometer show periodical structures which we interpret as internal gravity waves. Compositional effects are frequently seen in the data, in which the wave structures in different constituents show different amplitudes and phase angles. We use a simple linearized wave perturbation theory to explain the observations, emphasizing their role as a useful diagnostic of the basic wave parameters. For the T39 flyby, the data-model comparison constrains typical wavelength to be ~150–500 km, typical wave period from the Brunt-Väisälä period of ~62 min up to ~6 h. Our calculations also illustrate that wave-induced diffusion is important for CH_4 and H_2. **Citation:** Cui, J., Y. Lian, and I. C. F. Müller-Wodarg (2013), Compositional effects in Titan's thermospheric gravity waves, *Geophys. Res. Lett.*, *40*, 43–47, doi:10.1029/2012GL054621.

1. Introduction

[2] Gravity wave structures in planetary neutral atmospheres have been extensively studied on various Solar System bodies such as Earth [*Newton et al*., 1969; *Potter et al*., 1976], Jupiter [*Young et al*., 1997], Mars [*Fritts et al*., 2006; *Creasey et al*., 2006], and Venus [*Gierasch*, 1987; *Kasprzak et al*., 1988; *Hinson and Jenkins*, 1995]. For Titan, the largest satellite of Saturn, early evidences for wave structures in its neutral atmosphere are based on either the Voyager radio occultation data [*Hinson and Tyler*, 1983; *Friedson*, 1994] or the ground-based observations of stellar occultations [*Sicardy et al*., 1999, 2006]. More recently, the Huygens Atmospheric Structure Instrument (HASI) data revealed the presence of wave-like perturbations from as low as the stratopause to the exo-base region [*Fulchignoni et al*., 2005]. Further evidences were provided by the Cassini measurements made with either the Ion Neutral Mass Spectrometer (INMS) [*Müller-Wodarg et al*., 2006] (hereafter, MW06) or the UltraViolet Imaging Spectrograph (UVIS) [*Koskinen et al*., 2011].

[3] Of our particular interest here is the finding of MW06 that the wave structures of the two most abundant constituents in Titan's atmosphere, N_2 and CH_4, exhibit different amplitudes and phase angles, but no interpretation was given in that study. Such compositional effects are known to exist both on Earth [*Reber et al*., 1975] and on Venus [*Kasprzak et al*., 1993]. For example, *Reber et al*. [1975] showed that the fractional Ar (He) density variations in the terrestrial thermosphere were about twice (half) as large as the fractional N_2 density variations and that the He variations were in general 180° out of phase with both the N_2 and Ar variations. Here we investigate similar phenomena on Titan. In addition to the two constituents discussed in MW06, we also include H_2 and $^{29}N_2$ in our analysis. The observations are presented in section 2, followed by interpretations in section 3. Finally, we conclude and discuss in section 4.

2. Observations

[4] The analysis presented here is based on the Cassini INMS N_2, CH_4, H_2, and $^{29}N_2$ data obtained from the Planetary Plasma Interactions (PPI) node of the NASA Planetary Data System (PDS) public archives (http://ppi.pds.nasa.gov), including 24 flybys from T5 (on 16 April 2005) to T71 (on 7 July 2010). The data are reduced in a way similar to our previous works in *Müller-Wodarg et al*. [2008] and *Cui et al*. [2008, 2009] but also incorporating the improved algorithms described in *Cui et al*. [2012]. For each constituent (denoted with subscript i), we subtract the large scale trend, n_i, from the raw INMS density, $n_{i,\mathrm{obs}}$, where n_i is extracted from a fourth-order polynomial fitting to logarithmic $n_{i,\mathrm{obs}}$ as a function of time from closest approach (hereafter, CA). We then calculate the normalized residual density, defined as $\delta n_i/n_i = (n_{i,\mathrm{obs}} - n_i)/n_i$, for each constituent.

[5] For illustrative purpose, we take T39 as an example in the following discussions. This is a typical INMS-favored flyby on 20 Dec 2007 with CA occurring at 970 km, at the dayside, at the anti-Saturn and southern high latitude regions, and under plasma-sheet conditions [*Rymer et al*., 2009]. The normalized residual density for this flyby is shown in Figure 1 as a function of time from CA. The figure reveals the presence of wave-like structures in all constituents. Roughly speaking, one full periodical structure is seen within the time interval from approximately –250 s to CA or from CA to approximately +250 s, implying an observed wavelength of $\lambda_{\mathrm{obs}} \sim 1500$ km along the spacecraft trajectory (with a typical spacecraft velocity of 6 km s^{-1}) [*Cui et al*., 2009]. This serves as an upper limit to the true wavelength, λ.

[6] Compositional effects, in terms of both wave amplitude and phase angle, are clearly seen in Figure 1. Visual inspection of the full periodical structures from –250 s to +250 s suggests wave amplitudes to be ~0.2–0.3 for N_2, ~0.05–0.15 for CH_4, ~0.07–0.15 for H_2, and ~0.2–0.4 for $^{29}N_2$. Accordingly, the CH_4-N_2 amplitude ratio is ~0.25–0.5, the H_2-N_2 amplitude ratio is ~0.35–0.5, and the $^{29}N_2$-N_2 amplitude ratio is ~1–1.3. The vertical dashed lines in Figure 1 mark the positions of wave peaks near +150 s from CA, revealing that the wave structures in minor constituents are roughly in phase with the N_2 wave structure. For CH_4-N_2

[1]School of Astronomy and Space Sciences, Nanjing University, Nanjing, China.
[2]Ashima Research, Pasadena, California, USA.
[3]Department of Physics, Imperial College, London, UK.

Corresponding author: J. Cui, School of Astronomy and Space Sciences, Nanjing University, Nanjing 210018, China. (jcui@nju.edu.cn)

0094-8276/13/2012GL054621

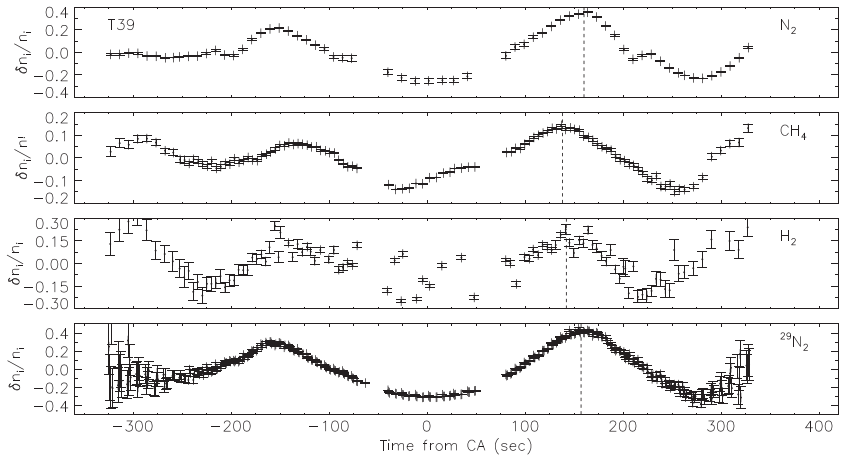

Figure 1. The residual density for constituent i (N_2, CH_4, H_2, and $^{29}N_2$), $\delta n_i/n_i$ as a function of time from CA for the T39 flyby. The residual density is calculated by subtracting the large scale density trend, n_i, from the raw INMS density, which is then normalized by n_i. The figure reveals periodical structures in all constituents, with the vertical dashed lines giving the positions of wave peaks to facilitate relative phase comparison. Compositional effects, in terms of both wave amplitude and phase angle, are clearly seen.

and H_2-N_2, the absolute phase differences are ~20 s in time from CA or equivalently ~30° in phase angle. For comparison, the $^{29}N_2$-N_2 phase difference is smaller, ~3 s in time from CA or ~4° in phase angle. The uncertainty in phase difference is difficult to estimate quantitatively, and we expect it to be primarily associated with the fact that the phase difference is not always constant along the spacecraft trajectory. This probably implies more than one wave train in the observed wave structure (e.g., MW06). For illustrative purpose, we assume a 10% uncertainty for phase difference in the model-data comparison to be presented below.

3. Interpretations

[7] For constituent i, we use p_i, ρ_i to denote the pressure and density of the unperturbed, background component, respectively, and we use p_i', ρ_i', u_i', and w_i' to denote the pressure, density, and the horizontal and vertical velocities of the perturbed component, respectively. We adopt normal mode solutions to $\delta p = p_i'/p_i$, $\delta\rho = \rho_i'/\rho_i$, u_i', and w_i' with the form of $\exp(z/2H_i)\exp[i(\Omega t - lx - kz)]$, where x and z are the horizontal and vertical coordinates, respectively, l and k are the corresponding wave numbers, Ω is the wave frequency, and H_i is the vertical pressure scale height. The linearized wave equations for N_2 (denoted with subscript 0 hereafter) can be written as

$$i\Omega\frac{\tilde{\rho}_0}{\rho_0} - il\tilde{u}_0 - \left(\frac{1}{2H_0} + ik\right)\tilde{w}_0 = 0, \tag{1}$$

$$i\Omega\tilde{u}_0 - il\frac{c_0^2}{\gamma}\frac{\tilde{p}_0}{p_0} = 0, \tag{2}$$

$$i\Omega\tilde{w}_0 - \left(\frac{1}{2H_0} + ik\right)\frac{c_0^2}{\gamma}\frac{\tilde{p}_0}{p_0} + \frac{\tilde{\rho}_0}{\rho_0}g = 0, \tag{3}$$

and

$$i\Omega\frac{\tilde{p}_0}{p_0} - \frac{\tilde{w}_0}{H_0} = \gamma\left(i\Omega\frac{\tilde{\rho}_0}{\rho_0} - \frac{\tilde{w}_0}{H_0}\right), \tag{4}$$

where γ is the ratio of specific heats (taken to be 1.4 for all constituents); g is the local gravity; $c_0^2 = \gamma g H_0$ with c_0 being the speed of sound; and $\tilde{p}_0$, $\tilde{\rho}_0$, $\tilde{u}_0$, and $\tilde{w}_0$ are complex constants given by the polarization relations [*Hines*, 1960]. Equations (1)–(4) lead to the well-known dispersion relation of

$$\left(\Omega^2 - \Omega_a^2\right)\frac{\Omega^2}{c_0^2} - \Omega^2\left(l^2 + k^2\right) + \Omega_b^2 l^2 = 0, \tag{5}$$

where $\Omega_a = \gamma g/2c_0$ is the acoustic cutoff frequency and $\Omega_b = (\gamma - 1)^{1/2} g/c_0$ is the Brunt-Väisälä frequency [*Hines*, 1960]. Two branches of normal wave mode are implied by equation 5, one for acoustic waves with $\Omega > \Omega_a$ and the other one for internal gravity waves with $\Omega < \Omega_b$. For T39 and at a reference altitude of 1250 km, $g \sim 60\ \mathrm{cm\,s^{-2}}$, $H_0 \sim 60$ km, $c_0 \sim 2.3 \times 10^4\ \mathrm{cm\,s^{-1}}$, and thus $\Omega_a \sim 1.9 \times 10^{-3}$ Hz and $\Omega_b \sim 1.7 \times 10^{-3}$ Hz, corresponding to wave periods of $\tau_a = 2\pi/\Omega_a \sim 55$ min and $\tau_b = 2\pi/\Omega_b \sim 62$ min, respectively. The gap between Ω_a and Ω_b contains no real normal mode wave solutions.

[8] For a minor constituent (CH_4, H_2, or $^{29}N_2$, denoted with subscript 1 hereafter), we include wave-induced diffusion [e.g., *Del Genio et al.*, 1979] as the diffusion time constant (typically several hours) might be comparable with the wave period (see below). Accordingly, the linearized momentum equations for perturbations in a minor constituent are

$$i\Omega\tilde{u}_1 - il\frac{c_1^2}{\gamma_1}\frac{\tilde{p}_1}{p_1} = -\nu_1(\tilde{u}_1 - \tilde{u}_0), \tag{6}$$

and

$$i\Omega\tilde{w}_1 - \left(\frac{1}{2H_1} + ik\right)\frac{c_1^2}{\gamma_1}\frac{\tilde{p}_1}{p_1} + \frac{\tilde{\rho}_1}{\rho_1}g = -\nu_1(\tilde{w}_1 - \tilde{w}_0), \tag{7}$$

where ν_1 is the collision frequency of the minor constituent diffusing through the background N_2 gas. The linearized continuity and energy equations are the same as equations (1) and (4) except for a change in subscript. For T39, the observed scale heights for the minor constituents are ~90 km for CH_4, ~120 km for H_2, and ~55 km for $^{29}N_2$, respectively.

[9] Several implicit assumptions in the above formulism need to be emphasized. (1) Similar to *Hines* [1960], the background component is taken to be stationary and isothermal for simplicity. In the case with a constant background

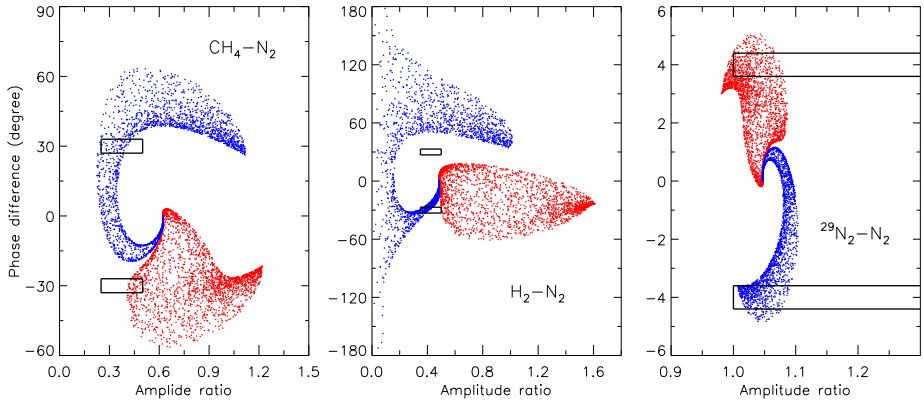

Figure 2. The distribution of 5000 random realizations of internal gravity waves in terms of amplitude ratio and phase difference, for various constituents in Titan's upper atmosphere. The solid box in each panel gives the region constrained by the T39 data. The sign of the phase difference depends on how the horizontal axis is defined; thus, only the magnitude is of interest here. Red and blue symbols in the figure represent waves with positive and negative vertical wave numbers, respectively. The data-model comparison constrains the wave structures seen in the T39 INMS data to be internal gravity waves with typical wavelengths of ~150–500 km and typical wave periods from the Brunt-Väisälä period of ~62 min up to ~6 h.

horizontal wind field, the wave frequency, **Ω**, should be interpreted as the intrinsic wave frequency [e.g., *Pitteway and Hines*, 1965]. (2) Adopting the normal mode solution implies that both gravity and collision frequency are assumed to be independent of altitude. As stated in *Del Genio et al.* [1979], this greatly simplifies the problem but still retains the basic features of the wave solution. (3) We have assumed a common temperature perturbation for all constituents, implying no net energy transfer from N_2 to a minor constituent via collision [*Del Genio et al.*, 1979, equation 3]. It can be verified that in order of magnitude, the ratio of the temperature difference to the background temperature is given by the multiplication of Ω/ν_1 with $\delta\rho_1'/\rho_1$. For T39 and at 1250 km, we estimate the collision frequency, ν_1, to be ~0.04–0.2 Hz for different minor constituents. Thus, the temperature difference can be safely ignored for all waves with periods much longer than several minutes. This is qualitatively consistent with the finding of *Del Genio et al.* [1979] that the temperature difference is generally negligible except for the short period end of the acoustic wave branch (see their Figure 12). (4) By ignoring the collisional terms in the momentum and energy equations for the N_2 perturbations, the minor mode solutions are naturally removed. This is a desired situation as minor mode solutions usually have unrealistically large wave amplitudes [e.g., *Del Genio et al.*, 1979].

[10] To interpret the observed compositional effects, we throw 100,000 random pairs of uniformly distributed horizontal and vertical wavelengths, λ_x and λ_z, to parametrize the possible range of normal wave modes. For each random realization, we require that the true wavelength, $\lambda = \left(1/\lambda_x^2 + 1/\lambda_z^2\right)^{-1/2}$, is no larger than 1500 km (see section 2). The horizontal and vertical wave numbers, $l = 2\pi/\lambda_x$ and $k = 2\pi/\lambda_z$, are used to calculate the corresponding wave periods with equation 5, for both the acoustic wave branch and the internal gravity wave branch. The linearized wave equations are then solved to determine the properties of the wave structures for different constituents.

[11] The distribution of the above random realizations in terms of the amplitude ratio and phase difference is illustrated in Figure 2, with the solid box in each panel giving the region constrained by the T39 data. We note that only the magnitude of the phase difference is of interest here, as the exact sign of the calculated phase difference depends on how the horizontal axis is defined. To improve visibility, only 5000 random realizations are shown in this figure (and Figure 3 below). The red and blue symbols represent internal gravity waves with positive and negative vertical wave numbers, respectively. Their distinction reflects the inherent vertical anisotropy of the background atmosphere and is expected to vanish in the limit of vertical wavelength much shorter than the scale height. From the figure, the calculated CH_4-N_2 amplitude ratio is in the range of ~0.2–1.2, and the corresponding phase difference is generally between ±60°. For H_2 and N_2, their amplitude ratio covers a wide range from negligibly small to ~1.6, and their phase difference occupies the full 2π range. The $^{29}N_2$-N_2 amplitude ratio is

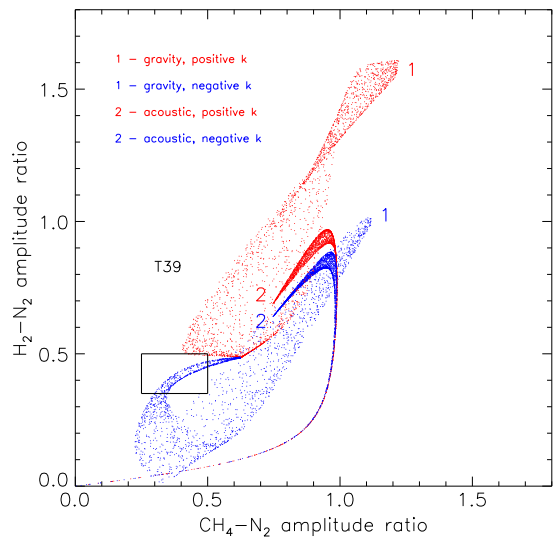

Figure 3. The distribution of 5000 random realizations of both acoustic and internal gravity wave modes, in terms of the CH_4-N_2 and H_2-N_2 amplitude ratios appropriate for the T39 flyby. Red and blue symbols account for positive and negative k modes, respectively. The solid rectangle marks the region allowed by the INMS observation.

restricted to a narrow range near ~1.1, and the phase difference is within ±5°. For both the CH_4-N_2 and H_2-N_2 compositional effects, positive k modes tend to have smaller phase differences than negative k modes. The denseness of the model points in each panel of Figure 2 does not necessarily reflect the actual probability distribution, as the model calculations are based on the assumption of uniformly distributed horizontal and vertical wavelengths. Instead, the envelop of the model points is more instructive, giving the possible ranges of amplitude ratio and phase difference. The values of these parameters implied by the T39 data (see section 2) are encompassed within the model ranges. The tendency of a larger amplitude ratio and a smaller phase difference for $^{29}N_2$-N_2 as compared to CH_4-N_2 or H_2-N_2 is well reproduced by our simplified model.

[12] The behaviors for the CH_4-N_2 and H_2-N_2 compositional effects are especially interesting. The T39 observations suggest CH_4-N_2 amplitude ratio of ~0.25–0.5 and H_2-N_2 amplitude ratio of ~0.35–0.5. For comparison, we show in Figure 3 the distribution of the random realizations of normal wave modes in terms of the above two amplitude ratios. The red and blue symbols indicate positive and negative vertical wave numbers, respectively. Both the internal gravity wave branch and the acoustic wave branch are shown, but the latter is clearly in conflict with the observations indicating the perturbations seen in the data cannot be acoustic in nature. To determine more rigorously the allowed values of wavelength and wave period, we require that the calculated amplitude ratios be within the observed ranges, as indicated by the solid rectangle in Figure 3. These criteria constrain the possible range of wavelength to be 150–500 km, and the possible intrinsic wave period from the Brunt-Väisälä period up to ~6 hr.

[13] As stated in *Del Genio et al*. [1979], the density variations due to waves are the combined result of adiabatic expansion and vertical advection (see equation 1). In the limit of negligible wave-induced diffusion [*Dudis and Reber*, 1976], the former is common to all constituents but the latter depends on the respective vertical distribution and is inversely proportional to the scale height. For illustrative purpose, we consider positive k modes: For constituents with scale heights smaller than the N_2 scale height (e.g., $^{29}N_2$), vertical advection from below (that causes density increase) dominates adiabatic expansion (that causes density decrease), leading to enhanced amplitudes as compared to N_2. In contrast, for constituents with scale heights larger than the N_2 scale height (e.g., CH_4 and H_2), vertical advection is not strong enough to counteract adiabatic expansion, thus leading to the opposite trend. A similar picture holds for the more complicated case with wave-induced diffusion being important, but now the effect of adiabatic expansion is no longer common to all constituents.

[14] To investigate the importance of wave-induced diffusion, we also calculate the amplitude ratios assuming identical perturbation velocities for all constituents, corresponding to infinite neutral collision frequencies in equations (6) and (7). For illustrative purpose, we consider the wave mode with an intrinsic wave period of 1.5 h and an overall wavelength of 170 km (with $l \sim 2.4 \times 10^{-7}\text{cm}^{-1}$, $k \sim 2.7 \times 10^{-7}\ \text{cm}^{-1}$). When wave-induced diffusion is ignored, the predicted CH_4-N_2 and H_2-N_2 amplitude ratios are ~0.4 and 0.25, different from the values of ~0.5 and 0.4 for the case with wave-induced diffusion included. However, the amplitude ratios for $^{29}N_2$-N_2 are nearly identical for the two cases. The above facts indicate that wave-induced diffusion is important for CH_4 and H_2 but negligibly small for $^{29}N_2$.

4. Discussions and Conclusions

[15] The Cassini INMS measurements of the density profiles of neutral constituents in Titan's upper atmosphere reveal periodical structures, which we interpret as internal gravity waves. In this study, we are particularly interested in the compositional effects of N_2, CH_4, H_2, and $^{29}N_2$ that are frequently seen in the data (see also MW06). Taking T39 as an example, we find that (1) the CH_4 and H_2 wave amplitudes tend to be smaller than the N_2 wave amplitude, but the $^{29}N_2$ wave amplitude tends to be larger, and (2) the wave structures in different constituents are roughly in phase, and the $^{29}N_2$-N_2 phase difference is in general smaller than the CH_4-N_2 and H_2-N_2 phase differences.

[16] We interpret the observed compositional effects with the linearized wave perturbation theory that also includes the effect of wave-induced diffusion [*Del Genio et al*., 1979]. To simplify the problem, we ignore the altitude dependence of gravity and collision frequency, and the calculations are made at a reference altitude of 1250 km. The data-model comparison indicates that the structures seen in the INMS data represent internal gravity waves with characteristic wavelengths of ~150–500 km and wave periods from the Brunt-Väisälä period of ~62 min up to ~6 h. We also assess the importance of wave-induced diffusion and find that it is important for CH_4 and H_2 but negligible for $^{29}N_2$.

[17] The model calculations presented in this study illustrate quantitatively how the amplitude ratio and phase difference in Titan's upper atmosphere could be interpreted with a simplified model. However, the characteristic wave parameters derived for T39 cannot be generalized to other flybys. For the bulk of the flybys showing wave structures in the upper atmosphere, the CH_4-N_2 amplitude ratio is in the range of ~0.3–1 with a mean of ~0.7, generally consistent with the model prediction presented here and with the variability at least partly due to the variable conditions in the background atmosphere [e.g., *Müller-Wodarg et al*., 2008; *Westlake et al*., 2011]. However, occasionally the CH_4-N_2 amplitude ratio could be as large as ~1.5, as for the case of the T5 flyby (MW06). This is significantly higher than the predicted value, illustrating the limitation of the simple linearized model presented here. Other important physical processes such as wave dissipation may need to be included to better reproduce the observations. For H_2-N_2, about a third of the flybys show amplitude ratios as large as >2, which we suspect to be a result of residual thruster firing contamination not properly removed in the data analysis [e.g., *Cui et al*., 2008]. The $^{29}N_2$-N_2 amplitude ratio is greater than 1 in all cases, an expected result as discussed in section 3.

[18] **Acknowledgments.** JC acknowledges support by the National Science Foundation of China through grant NSFC-41174146. YL is supported by the NASA Planetary Atmosphere Program NNX10AB99G. IMW is supported by the UK Science & Technology Facilities Council (STFC).

References

Creasey, J. E., J. M. Forbes, and G. M. Keating (2006), Density variability at scales typical of gravity waves observed in Mars' thermosphere by the MGS accelerometer, *Geophys. Res. Lett.*, *33*, L22814, doi:10.1029/2006GL027583.

Cui, J., R. V. Yelle, and K. Volk (2008), Distribution and escape of molecular hydrogen in Titan's thermosphere and exosphere, *J. Geophys. Res.*, *113*, E10004, doi:10.1029/2007JE003032.

Cui, J., et al. (2009), Analysis of Titan's neutral upper atmosphere from Cassini Ion Neutral Mass Spectrometer measurements, *Icarus*, *200*, 581–615, doi:10.1016/j.icarus.2008.12.005.

Cui, J., et al. (2012), The CH_4 structure in Titan's upper atmosphere revisited, *J. Geophys. Res.*, *117*, E11006, doi:10.1029/2012JE004222.

del Genio, A. D., G. Schubert, and J. M. Straus (1979), Characteristics of acoustic-gravity waves in a diffusively separated atmosphere, *J. Geophys. Res.*, *84*, 1865–1879, doi:10.1029/JA084iA05p01865.

Dudis, J. J., and C. A. Reber (1976), Composition effects in thermospheric gravity waves, *Geophys. Res. Lett.*, *3*, 727–730, doi:10.1029/GL003i012p00727.

Friedson, A. J. (1994), Gravity waves in Titan's atmosphere, *Icarus*, *109*, 40–57, doi:10.1006/icar.1994.1076.

Fritts, D. C., L. Wang, and R. H. Tolson (2006), Mean and gravity wave structures and variability in the Mars upper atmosphere inferred from Mars Global Surveyor and Mars Odyssey aerobraking densities, *J. Geophys. Res.*, *111*, A12304, doi:10.1029/2006JA011897.

Fulchignoni, M., et al. (2005), In situ measurements of the physical characteristics of Titan's environment, *Nature*, *438*, 785–791, doi:10.1038/nature04314.

Gierasch, P. J. (1987), Waves in the atmosphere of Venus, *Nature*, *328*, 510–512, doi:10.1038/328510a0.

Hines, C. O. (1960), Internal atmospheric gravity waves at ionospheric heights, *Can. J. Phys.*, *38*, 1441–1481, doi:10.1139/p60-150.

Hinson, D. P., and J. M. Jenkins (1995), Magellan radio occultation measurements of atmospheric waves on Venus, *Icarus*, *114*, 310–327, doi:10.1006/icar.1995.1064.

Hinson, D. P., and G. L. Tyler (1983), Internal gravity waves in Titan's atmosphere observed by Voyager radio occultation, *Icarus*, *54*, 337–352, doi:10.1016/0019-1035(83)90202-6.

Kasprzak, W. T., A. E. Hedin, H. G. Mayr, and H. B. Niemann (1988), Wavelike perturbations observed in the neutral thermosphere of Venus, *J. Geophys. Res.*, *93*, 11237–11245, doi:10.1029/JA093iA10p11237.

Kasprzak, W. T., H. B. Niemann, A. E. Hedin, and S. W. Bougher (1993), Wave-like perturbations observed at low altitudes by the Pioneer Venus Orbiter Neutral Mass Spectrometer during orbiter entry, *Geophys. Res. Lett.*, *20*, 2755–2758, doi:10.1029/93GL02628.

Koskinen, T. T., et al. (2011), The mesosphere and thermosphere of Titan revealed by Cassini/UVIS stellar occultations, *Icarus*, *216*, 507–534, doi:10.1016/j.icarus.2011.09.022.

Müller-Wodarg, I. C. F., R. V. Yelle, N. Borggren, and J. H. Waite Jr. (2006), Waves and horizontal structures in Titan's thermosphere, *J. Geophys. Res.*, *111*, A12315, doi:10.1029/2006JA011961.

Müller-Wodarg, I. C. F., R. V. Yelle, J. Cui, and J. H. Waite Jr. (2008), Horizontal structures and dynamics of Titan's thermosphere, *J. Geophys. Res.*, *113*, E10005, doi:10.1029/2007JE003033.

Newton, G. P., D. T. Peiz, and H. Volland (1969), Direct in situ measurements of wave propagation in the neutral thermosphere, *J. Geophys. Res.*, *74*, 183–196, doi:10.1029/JA074i001p00183.

Pitteway, M. L. V., and C. O. Hines (1965), The reflection and ducting of atmospheric acoustic-gravity waves, *Can. J. Phys.*, *43*, 2222–2243, doi:10.1139/p65-217.

Potter, W. E., D. C. Kayser, and K. Mauersberger (1976), Direct measurements of neutral wave characteristics in the thermosphere, *J. Geophys. Res.*, *81*, doi:10.1029/JA081i028p05002.

Reber, C. A., A. E. Hedin, D. T. Pelz, L. H. Brace, and W. E. Potter (1975), Phase and amplitude relationships of wave structure observed in the lower thermosphere, *J. Geophys. Res.*, *80*, 4576–4580, doi:10.1029/JA080i034p04576.

Rymer, A. M., H. T. Smith, A. Wellbrock, A. J. Coates, and D. T. Young (2009), Discrete classification and electron energy spectra of Titan's varied magnetospheric environment, *Geophys. Res. Lett.*, *36*, L15109, doi:10.1029/2009GL039427.

Sicardy, B., et al. (1999), The structure of Titan's stratosphere from the 28 Sgr occultation, *Icarus*, *142*, 357–390, doi:10.1006/icar.1999.6219.

Sicardy, B., et al. (2006), The two Titan stellar occultations of 14 November 2003, *J. Geophys. Res.*, *111*, E11S91, doi:10.1029/2005JE002624.

Westlake, J. H., et al. (2011), Titan's thermospheric response to various plasma environments, *J. Geophys. Res.*, *116*, A03318, doi:10.1029/2010JA016251.

Young, L. A., R. V. Yelle, R. Young, A. Seiff, and D. B. Kirk (1997), Gravity waves in Jupiter's thermosphere, *Science*, *276*, 108–111, doi:10.1126/science.276.5309.108.